



저작자표시-비영리-변경금지 2.0 대한민국

이용자는 아래의 조건을 따르는 경우에 한하여 자유롭게

- 이 저작물을 복제, 배포, 전송, 전시, 공연 및 방송할 수 있습니다.

다음과 같은 조건을 따라야 합니다:



저작자표시. 귀하는 원저작자를 표시하여야 합니다.



비영리. 귀하는 이 저작물을 영리 목적으로 이용할 수 없습니다.



변경금지. 귀하는 이 저작물을 개작, 변형 또는 가공할 수 없습니다.

- 귀하는, 이 저작물의 재이용이나 배포의 경우, 이 저작물에 적용된 이용허락조건을 명확하게 나타내어야 합니다.
- 저작권자로부터 별도의 허가를 받으면 이러한 조건들은 적용되지 않습니다.

저작권법에 따른 이용자의 권리는 위의 내용에 의하여 영향을 받지 않습니다.

이것은 [이용허락규약\(Legal Code\)](#)을 이해하기 쉽게 요약한 것입니다.

[Disclaimer](#)

Doctor of Philosophy

EVALUATION OF THE FEASIBILITY OF  
A NOVEL SWINE MODEL FOR  
EMPTY NOSE SYNDROME  
USING HISTOLOGIC EXAMINATION AND  
COMPUTATIONAL FLUID DYNAMICS

돼지를 이용한 빈코 증후군의 동물 모델 개발과  
조직학적 분석과 전산 유체 역학 분석을 통한 효용성 평가

The Graduate School  
of the University of Ulsan  
Department of Otolaryngology  
Shin Ae Kim

EVALUATION OF THE FEASIBILITY OF  
A NOVEL SWINE MODEL FOR  
EMPTY NOSE SYNDROME  
USING HISTOLOGIC EXAMINATION AND  
COMPUTATIONAL FLUID DYNAMICS

Supervisor: Yong Ju Jang.

A Dissertation

Submitted to  
the Graduate School of the University of Ulsan  
In Partial Fulfillment of the Requirements  
for the Degree of

Doctor of Philosophy

by

Shin Ae Kim

Department of Otolaryngology,  
University of Ulsan, South Korea  
February 2024

EVALUATION OF THE FEASIBILITY OF  
A NOVEL SWINE MODEL FOR  
EMPTY NOSE SYNDROME  
USING HISTOLOGIC EXAMINATION AND  
COMPUTATIONAL FLUID DYNAMICS

This certifies that the dissertation thesis  
of Shin Ae Kim is approved.

Chung, Yoo-Sam

Committee Chair Dr.

Jang, Yong Ju

Committee Member Dr.

Kim, Ji Sun

Committee Member Dr.

Yu, Myeong Sang

Committee Member Dr.

Kim, Ji Heui

Committee Member Dr.

Department of Otolaryngology,  
University of Ulsan, South Korea

February 2024

## 감사의 글

독창적이고 창의적인 이 프로젝트를 할 수 있는 영광을 주신 지도교수님 장용주 교수님께 깊은 존경과 감사의 마음을 전합니다. 항상 틀에 얽매이지 않는 사고로 논문 작성 과정에서도 많은 깨달음을 주셨습니다. 공사다망 하심에도 흔쾌히 논문의 심사위원장을 맡아 주신 정유삼 교수님, 심사위원을 맡아 주신 김지선 교수님, 유명상 교수님, 김지희 교수님도 항상 뒤에서 지켜봐 주시고 언제나 든든한 지지를 아끼지 않으셨습니다.

또한 연구 내용 전반에서 아낌없는 도움을 주신 분들께 깊은 감사의 인사를 전합니다. 축산시장에 동행해주신 이병돈 교수님, 병리 조언을 해 주신 최인호 교수님, CFD 분석을 해 주신 나양 교수님, 대 동물 영상 검사를 가능하게 해 주신 영상의학과 임현경 교수님, 바쁜 당직 시간에도 흔쾌히 영상 촬영을 도와 주신 순천향대학교 서울병원 영상의학팀 그리고 돼지 검체 채취를 도와 주신 서울 아산병원 펠로우 선생님들께도 감사의 인사를 드립니다.

그리고 연구 기간 내내 저를 응원해 주신 우리 순천향대학교 서울병원 이비인후과학교실 선생님들께 진심으로 감사드립니다. 선생님들의 아낌없는 조언과 지지는 이 논문을 완성하는 데에 큰 힘이 되었습니다.

마지막으로, 논문을 작성하는 동안 아이를 돌봐 주시고 지원해주신 가족들에게도 감사의 인사를 전합니다. 부모님, 사랑하는 남편, 그리고 엄마 뱃속에서부터 실험과정을 함께한 우리 아이들, 민혁이, 시윤이에게 사랑의 마음을 전합니다.

## ENGLISH ABSTRACT

**Background.** Empty Nose Syndrome (ENS) is an iatrogenic condition that occurs after turbinate reduction surgery. The ENS has a complicated pathophysiology that requires extensive basic research. Recent studies suspected that decreased airflow sensation is related to a receptor that perceive cool sensation, and by analyzing computed tomography (CT) scans of the patients, there were decreased air-conditioning functions in the ENS patients. A good animal model would be a stepping stone for a better understanding of the pathogenesis and the development of treatment methods for this complicated condition; however, no relevant animal model of ENS has yet been established. Thus, this study aimed to develop a swine model of ENS and validate the feasibility of this model using histological and Computational Fluid Dynamics (CFD) analyses.

**Methods.** Four Yorkshire pigs underwent unilateral turbinectomy and were sacrificed 6 months postoperatively. Both nasal mucosal linings were harvested and histological analysis was performed using Hematoxylin and Eosin (H&E), S-100, Transient Receptor Potential channel subfamily M member 8 (TRPM-8) receptor, Transient Receptor Potential Vanilloid 1 (TRPV1), and Piezo-type mechanosensitive ion channel component 2 (PIEZO2) stainings.

A CFD analysis was also performed on Yorkshire pigs to validate the ENS model in terms of airflow characteristics. Computed Tomography (CT) scans of the entire pig head were performed preoperatively and after unilateral and bilateral turbinate resection.

**Results.** Compared to the control mucosa, H&E staining of the ENS swine model showed significantly increased squamous metaplasia in the anterior portion (positivity rate, 96.4% vs. 78.6%,  $p=0.043$ ) and submucosal fibrosis in the middle portion (positivity rate, 42.9% vs. 17.9%,  $p=0.018$ ). There were no neuronal inflammatory changes on S-100 staining; however, there was a marked decrease in TRPM-8 expression in the peripheral nerves (positivity rate, 50.0% vs. 95.3%,

p=0.010). TRPV1 staining showed an overall increase in expression levels in peripheral nerves (positivity rate, 71.4% vs. 14.3, p=0.025). CFD analysis showed decreased overall nasal resistance and decreased relative humidity and air temperature at the choana level, similar to the changes found in human CFD data for ENS.

**Conclusions.** Pathologic features, changes in the level of TRP receptors and the CFD changes indicate that the ENS swine model could serve as a feasible animal model to better understand the pathophysiology of ENS.

**Keywords.** turbinates, atrophic rhinitis, transient receptor potential channels, iatrogenic disease, nasal surgery

## CONTENTS

|  |    |
|--|----|
| ENGLISH ABSTRACT .....                         | 4  |
| LIST OF TABLES.....                            | 7  |
| LIST OF FIGURES .....                          | 8  |
| INTRODUCTION .....                             | 9  |
| MATERIALS AND METHODS                          |    |
| 1. Surgery and mucosal harvest .....           | 13 |
| 2. Histological analysis .....                 | 14 |
| 3. Computed Fluid Dynamics (CFD) Analysis..... | 16 |
| 4. Statistical Analysis.....                   | 17 |
| RESULTS .....                                  | 19 |
| DISCUSSION .....                               | 23 |
| CONCLUSION.....                                | 29 |
| REFERENCES .....                               | 30 |
| KOREAN ABSTRACT .....                          | 46 |

## LIST OF TABLES

|  |    |
|--|----|
| <b>Table 1.</b> Summary of histologic findings on H&E staining. ....           | 34 |
| <b>Table 2.</b> Summary of quantitative analysis of immunohistochemistry ..... | 35 |
| <b>Table 3.</b> Preoperative and postoperative CFD calculation data. ....      | 36 |

## LIST OF FIGURES

**Figure 1.** A: Surgical view after harvesting the mucosa. B: Mucosal side of harvested specimens: post-turbinectomy site and control.....37

**Figure 2.** When the entire nasal mucosal specimen was harvested in a cylindrical shape, vertical sections were prepared for correlation with the coronal section of the CT scan. ....38

**Figure 3.** CT scan of a pig head. (A) Preoperative, (B) after left side unilateral inferior turbinectomy, (C) after bilateral inferior turbinectomy. .... 39

**Figure 4.** Numerical nasal cavity model..... 40

**Figure 5.** H&E-stained specimens of control (A, C) and ENS group. (B, D) In the lower-power view, the ENS group showed decreased mucosal glands (g) and submucosal fibrosis (asterisk) compared to the control group. (B) The mucosal lining of the ENS group was thickened and showed prominent squamous metaplasia. (D, arrow).....41

**Figure 6.** TRPM-8 levels in the peripheral nerves were decreased, whereas they were present in the small nerves of the control group..... 42

**Figure 7.** Comparison of TRPV1 and PIEZO-2 levels in control and ENS models. TRPV1 staining was prominent in the cytoplasm of ENS model nerve fibers. PIEZO-2 staining was mildly increased in the cytoplasm of ENS model nerve fibers. ....43

**Figure 8.** CFD analysis of the ENS model regarding streamline pattern, velocity distribution, relative humidity distribution, wall shear stress, and wall heat flux. The ENS model showed airflow centered in the middle third of the nasal cavity, increased air velocity throughout the nasal passage, especially in the middle third, decreased relative humidity, increased wall shear stress, and increased wall heat flux. .... 44

## INTRODUCTION

Empty Nose Syndrome (ENS) is an iatrogenic condition that occurs after turbinate surgery, with clinical symptoms including paradoxical nasal obstruction, nasal dryness, burning sensation, and respiratory discomfort.<sup>1</sup> This disease was first described in 1994, but initially, it did not receive much attention from many doctors, and patients with these symptoms were sometimes dismissed as having psychological issues.<sup>2,3</sup> However, a significant number of patients with ENS experience profound disabling symptoms, and a substantial portion of these patients even have suicidal ideation because of the nasal symptoms.<sup>4</sup> Moreover, formerly perceived as an exceedingly rare condition, recent research suggests that ENS may occur in as many as 8–22% of cases following turbinate resection surgery.<sup>5</sup> As awareness of ENS spreads, the diagnosis is on the rise, highlighting that it is more common than previously believed. ENS can be a source of dispute between doctors and patients, as it primarily arises after surgery, but not all patients who undergo turbinate resection develop the syndrome.<sup>6</sup> Even when surgery is performed with a focus on preserving the nasal structure, some patients still experience ENS, and the exact cause remains unclear, fueling the debate surrounding the functional role of turbinate surgery.<sup>5</sup>

Elucidating the pathophysiology of this condition may shed light on which aspects of current surgical techniques may be problematic and how to prevent ENS resulting from nasal surgery. However, there is a shortage of studies on the pathology of the disease, partly due to the reluctance of patients toward nasal mucosal biopsies and other invasive procedures, which makes it challenging to investigate the pathophysiology of the disease. Therefore, in the study of ENS, having an

appropriate animal model would be highly beneficial not only for a better understanding of the pathophysiology, but also for developing better treatment strategies, but the current reality is that there are no available models. Given the need for an animal model with a nasal structure similar to that of humans, we chose pigs as the candidate animal because they have round nostrils and spacious nasal passages similar to those of humans.<sup>7</sup>

While there is much more to uncover regarding the pathophysiology of ENS, two major pathophysiological characteristics of this disease have been highlighted. First, there is a diminished sense of airflow. When airflow occurs in the nasal cavity, it causes the evaporation of secretions lining the mucosa, which then extract heat from the mucosal surface, leading to a cool sensation. The receptor responsible for this cold sensation is the Transient Receptor Potential Melastatin 8 (TRPM8) ion channel. Distributed in the trigeminal nerve, TRPM8 responds to cool stimuli in the range of 8–28°C, generating action potentials and thereby detecting airflow.<sup>8,9</sup> The paradoxical obstruction symptoms of ENS are thought to arise from insufficient mucosal cooling and a reduction in the number of TRPM8 receptors due to surgery, hindering the effective functionality of TRPM8.<sup>3</sup>

In addition to the paradoxical nasal stuffiness, other symptoms such as pain, burning sensation, and suffocation cannot be fully explained by the decreased function of TRPM8. Therefore, we investigated the other sensory receptors that may be responsible for these symptoms. Receptors suspected to be relevant include transient receptor potential cation channel subfamily V member 1 (TRPV1: pain and heat receptor) and Piezo-type mechanosensitive ion channel component 2 (PIEZO2: pressure receptor).<sup>10</sup> TRPV1 perceives capsaicin, pain, and noxious heat and it could be related to “burning pain,” which is a typical characteristic of pain in patients with ENS. In contrast, PIEZO2 is known to play an important role in breathing perception

in the lungs as a pressure sensor, and the altered function of PIEZO2 in the lungs could induce suffocation. As ENS symptoms include paradoxical suffocation and a decrease in nasal resistance in patients with ENS, the pressure sensor TRPV1 and mechanoreceptor PIEZO2 should be investigated in this disease entity.

Notably, TRPM8, PIEZO2, and TRPV1 are found not only in nerve cells but also in various other cell types in the nasal mucosa. They are believed to act as ion channels in various tissues. Although the specific effects of these are still under investigation, it is thought that these channels may contribute to sensing various sensations and controlling the functions of tissues, not only in the neural system but also within the tissues themselves.<sup>11</sup> Therefore, we aimed to investigate how these ion channels are distributed in the nasal mucosal tissue and nerves of the pig model.

A decline in nasal air-conditioning function plays a significant role in the pathogenesis of ENS. Turbinates play a vital role in dispersing the airflow by creating an effective laminar flow for the exchange of temperature and moisture on the mucosal surface. The removal of turbinates not only reduces the mucosal surface area available for conditioning inhaled air but also disrupts the airflow pattern, diminishing the overall capacity to regulate the temperature and humidity of the inspired air. Recently, a model for predicting nasal temperature and humidity was developed using virtual computed fluid dynamics (CFD) analysis of patient CT scans. This model has become an actively utilized tool in ENS research, revealing reduced air conditioning function in patients with ENS regarding temperature and humidity regulation.<sup>12</sup> Furthermore, changes in airflow are suggested to be associated with the pathophysiology of ENS in a more complex way than simple deterioration of air conditioning functionality. According to recent studies, even with the same turbinectomy procedure, the likelihood of ENS occurrence is higher in the group where the inferior flow has decreased.<sup>13,14</sup> Therefore, in this study, we aimed to

investigate the air-conditioning parameters and airflow patterns through CFD analysis of the model.

Herein, we present our attempt to create a swine ENS model, validate it by its pathologic and CFD features, and disclose its relationship with sensory channels, TRPM8, TRPV1, and PIEZO-2, with the aim of demonstrating the feasibility of the swine model.

## MATERIALS AND METHODS

### **Surgery and mucosal harvest**

Four Yorkshire pigs were used in the present study. General anesthesia was induced by injecting zolazepam with tiletamine (Zoletil<sup>®</sup>, Virbac, TX, USA) 5 mg/kg, and After laryngeal intubation, anesthesia was maintained with sevoflurane inhalation. In the prone position, all pigs underwent a single-sided turbinectomy on the left side. Endoscopic turbinectomy was performed using scissors and forceps. As the anterior-most part of the pig's turbinate continues with cartilaginous tissue, we ensured that the anterior-most cartilaginous part of the turbinate was included in the area of resection. During the procedure, bleeding was minimal, less than 10 cc. After turbinectomy, bleeding was controlled meticulously using epinephrine-soaked cotton pads and/or electric suction coagulators. No packing materials were used after the procedure, and antibiotics and analgesics were administered for 24 h.

After 6 months, all pigs were sacrificed using venous potassium chloride (KCl) injection under deep anesthesia with zolazepam and tiletamine 5 mg/kg. After sacrifice, the pigs were placed in a prone position, and a vertical skin incision was made at the midline of the face, starting from the intercanthal area to the tip of the nose, between the nostrils. At the nostril level, circular skin incisions were made on both nostrils. The skin flap was elevated to the supraperiosteal level of the nasal bone and cartilage. When the entire nasal bone and cartilage were exposed, they were removed using various dissectors and chisels, with care not to damage the mucosa. The entire mucosa was elevated from the septal cartilage, lateral nasal wall, and the nasal floor in the subperichondrial and subperiosteal planes. At the choana level, the elevated cylindrical mucosa was cut using scissors. Figure 1 shows the surgical view

after mucosal harvesting and harvested mucosal specimens. All study procedures were performed with maximal concern for the animal's rights, and all possible enrichment activities were given to the animals. This study was approved by the Institutional Animal Care and Use Committee of the Asan Medical Center (approval number: 2021-13-089).

### **Histopathological analysis**

Harvested mucosa was immediately fixed in 10% neutral-buffered formalin for more than 24 h. Mucosal specimens were cut vertically on each slide to represent the coronal view on the CT scan (Figure 2). Histological analysis was done using Hematoxylin and Eosin (H&E), S-100, periodic acid-Schiff (PAS), Alcian blue staining, and immunohistochemical staining was done using antibodies for Transient Receptor Potential channel subfamily M member 8 (TRPM-8) receptor (ab3243, Abcam, Cambridge, UK), transient receptor potential vanilloid 1 (TRPV1) (ab3487, Abcam, Cambridge, UK), and Piezo-type mechanosensitive ion channel component 2 (PIEZO2) (ab244349, Abcam, Cambridge, UK). Immunohistochemistry was performed using an automated system according to the manufacturer's instructions.

A structured review was conducted for the histological analysis. As we harvested the entire nasal cavity mucosa of pigs, we reviewed specimens from each group based on histological differences in nasal regions and variations in the distribution of various receptors of interest. First, we created slides in the coronal plane of the pigs' nasal cavity, allowing us to produce approximately 10 slides for each nasal cavity in the anterior-to-posterior direction (Figure 2). For each specimen, three slides were selected to represent the anterior, middle, and posterior parts of the nasal cavity. Microscopic findings from each slide were evaluated at seven different sites, including the superior, middle, and inferior portions of the septum. Assessment of the

lateral nasal wall involved examining the normal side at three specific locations: the most medial and lateral portions of the concha (on its outer and inner surfaces, respectively) and the lateral wall of the nasal cavity. On the normal side of the lateral wall, distinct locations were considered, including the most medial and lateral portions of the concha, as well as the junction between the concha and the nasal cavity lateral wall. On the surgical side, the superior, middle, and inferior portions were evaluated at three locations to ensure comparability with the septal conditions. The floor was assessed in its central area, with a focus on a representative location because this area has a limited surface area compared to other regions.

Parameters such as the presence of squamous metaplasia (not identified=0, present=1), fibrotic changes in subepithelial connective tissue (not identified=0, present=1), proliferation of subepithelial glands (atrophy or mild glands to stromal ratio <25%=0, glands to stromal ratio >25%=1), and the presence of atrophic changes (not identified=0, present=1) were assessed on low-power (x12.5 or x40) H&E slides. Confirmation was carried out at mid- to high-power (x100, x400) if necessary. The degree of inflammatory cell infiltration (none=0, present=1) and presence of atrophy in the lining epithelium were confirmed at high power in representative areas previously evaluated at low power.

Immunohistochemical results were quantitatively evaluated by manually counting the number of stained cells and the intensity of each stain. The expression strength was assessed using a scale of none=0, mild=1, moderate=2, and strong=3. The score ranged from 0 to 300 and was calculated by multiplying the value by the percentage of stained cells at 400x magnification. S-100-stained slides were reviewed with each immunostained slide to locate the nerve fibers. From each nerve, it was determined whether immunostaining occurred, and percentages of nerves immunostained among the total nerves were calculated.

## **CFD Analysis**

The CFD analysis was performed separately using three Yorkshire pig heads. To facilitate the scanning process, the pig heads were resected at the level of the C7 spine, preserving the upper airway up to the laryngeal level. CT scanning was done in an osteomeatal unit CT setting, with 0.625 mm thickness, using the CT scanning system of General Electrics healthcare™. CT was performed three times for each pig head: preoperatively, after unilateral turbinate resection, and after bilateral turbinate resection (Figure 3). The turbinectomy procedure was performed under an endoscopic view using the same steps as in the in vivo pig model mentioned above.

Three-dimensional computational models of the nasal cavities were created using preoperative (pre-op model) and postoperative CT scan images (two postoperative models: unilateral turbinectomy and bilateral turbinectomy) for each pig. Mimics v22.0 (Materialise, Leuven, Belgium) and Geomagic (3F Systems, Rock Hill, SC, USA) software were used to generate the 3-D volume cavity models, as shown in Figure 4. The paranasal sinuses were removed because they did not significantly affect the airflow distribution through the nasal cavity in the reference pig model.

The velocity, pressure, temperature, and relative humidity distributions in the nasal airway were obtained by solving the continuity, momentum, energy, and species transport equations for a mixture of air and water vapor using ANSYS/Fluent R22.2 (Canonsburg, PA, USA). No-slip and constant temperature boundary conditions were applied along the epithelial surface of the nasal cavity.

Further details of the numerical methodology can be found in Kim et al.<sup>15</sup> and Chung and Na.<sup>3,16,17</sup> To estimate the temperature along the surface, a thermocouple was used to measure the temperature at the anterior septum of both the reference pig and humans. It should be noted that the temperature was approximately 4.1°C higher

in the reference pig, and the average temperature during the inspiration period was assumed to be 36.7°C (i.e., 4.1°C higher than the human value of 32.6°C, as reported by Lindeman et al.).<sup>18</sup> Ambient conditions were assumed to be 25°C and 35% relative humidity.

The tidal volume of a pig is approximately 490–500 mL, comparable to that of humans. Therefore, the target bilateral inspiratory airflow rate during calm breathing was assumed to be 250 mL/s, which is the typical average airflow rate in humans during inspiration in the bilateral turbinectomy model. At this airflow, turbulent features were not significant; thus, a laminar flow regime was used.<sup>16,17</sup> It was decided that comparing airflows in preoperative and postoperative models would be more reasonable by maintaining the same breathing effort. Consequently, after the computation for the bilateral turbinectomy model, the transnasal pressure drops between the inlet and choana were measured, and the same pressure value was prescribed at the choana for the computations with the unilateral turbinectomy and preoperative models.

Polyhedral meshes combined with prism elements placed along the epithelial surface were used in the computation using Fluent Meshing 2021R2 (Canonsburg, PA, USA). A grid-independence study was conducted for the preoperative model, which revealed that approximately 6.7 million mesh elements could reasonably resolve the airflow fields. Therefore, the same mesh size function was maintained in the mesh generation procedure for all other cavity models.

### **Statistical analyses**

Statistical analyses were performed using IBM® SPSS® Statistics for Windows (version 22.0; (SPSS Inc., Chicago, IL, USA). To compare expression levels by immunohistochemistry, we conducted the Mann–Whitney U test. Categorical variables were

compared using the chi-squared test. Logistic regression was used to compare differences between subsites. For the CFD results, the mean and standard deviation were calculated, and a t-test was performed to compare the preoperative and postoperative (Both) mean values. Statistical significance was set at  $p < 0.05$ .

## RESULTS

### *Histological findings from in vivo model*

Table 1 and Figure 5 show the results of the histological features of both groups. Four individual study specimens were analyzed in three regions, anterior, middle, and posterior, and each region was divided into seven subsites, superior septum, middle septum, inferior septum, nasal floor, superior lateral wall, mid lateral wall, and inferior lateral wall. Histological features varied significantly among the anterior, middle, and posterior parts ( $p < 0.05$ ). In contrast, no significant differences were noted among subsites, such as the septal wall, lateral wall, and nasal floor, using logistic regression analysis.

Squamous metaplasia was notably prominent in the anterior part of the nasal cavity, with significantly higher occurrence in the ENS group (27 subsites) than in the control group (22 subsites) ( $p = 0.043$ ). However, almost no significant epithelial changes were observed in the mid-portion of the nasal cavity in either group. Chronic inflammation was not significantly different between the two groups. Submucosal fibrosis exhibited a notable difference in the middle portion, with the control group having 5 occurrences and the ENS model group having 12 occurrences, showing a significantly higher incidence in the ENS model ( $p = 0.018$ ). There were no significant differences in the submucosal glands or atrophic changes between the groups. S-100 staining revealed no neuronal inflammatory changes in either group.

TRPM-8 was generally well stained in the glands, vascular walls, epithelial cells, and nerves of the control group. Quantitative analysis revealed that the mean intensity values were higher in the control group (146.3) than in the ENS model (111.4). However, these differences were not statistically significant ( $p = 0.373$ ) (Table 2). Notably, as described in Figure 6, TRPM-8 was well-expressed in the large nerves in the deep areas and medium-to-small-sized nerves located at the peripheral side of

the mucosa of the control, whereas at the turbinectomy site, medium to small nerves did not express TRPM-8, and larger nerves more than 0.1 mm in size expressed some TRPM-8, but at a less intense level compared to the control. The corresponding nerve staining percentages of 95.3 in the control group and 50.0 in the ENS group were significantly different ( $p=0.010$ ).

TRPV1 was highly expressed in nerves, vessels, mucin, and surface epithelia of both groups. TRPV1 levels changed in the opposite direction to that of TRPM8. An increase in TRPV1 intensity was observed in the ENS group (189.9) compared to the control group (153.7), although these differences did not reach statistical significance ( $p=0.373$ ). In contrast, the nerve staining percentages of 14.3 (control group) and 71.4 (ENS group) displayed statistically significant differences ( $p=0.025$ ). Figure 7 shows increased TRPV1 levels in the nerve cytoplasm of the ENS model.

PIEZO-2 was stained in epithelial cells, capillary endothelial cells, and some glands but not in nerves. In PIEZO-2 staining, the mean intensity values increased in the ENS model (171.7) compared to those in the control group (100.6), but this difference was not statistically significant ( $p=0.126$ ). The corresponding nerve staining percentages also varied, with 0 in the control group and 10.7 in the ENS group, although this difference was not statistically significant ( $p=0.406$ ). Figure 7 shows mildly increased PIEZO-2 levels in the nerve cytoplasm of the ENS model.

### *CFD analysis results*

Table 3 presents the mean preoperative and postoperative CFD data for the three models. The average airflow rate in the right nostril was 55.6 mL/s (SD: 13.1) before surgery, 57.2 mL/s (SD: 12.2) after left-side surgery, and 130.1 mL/s (SD: 10.8) after bilateral surgery, showing a statistically significant difference before and after surgery ( $p=0.002$ ). In the left nostril, the average airflow rate was 53.3 mL/s (SD: 9.5) before surgery, 127.3 mL/s (SD: 14.8) after left-side surgery, and 121.8 mL/s (SD: 10.7) after bilateral surgery, with a statistically significant difference before and after surgery ( $p=0.001$ ). The flow partitioning between the right and left nostrils

showed no significant changes ( $p=0.778$ ).

The airflow rate from the nasal inlet was 107.6 mL/s (SD: 22.0) before surgery, 182.9 mL/s (SD: 9.4) after left-side surgery, and 250.0 mL/s (SD: 0.3) after bilateral surgery, with a significant difference before and after surgery ( $p<0.001$ ). Nasal resistance in both nostrils decreased from 0.077 Pa s/mL (SD: 0.043) before surgery, 0.041 Pa s/mL (SD: 0.015) after left side surgery, and 0.030 Pa s/mL (SD: 0.012) after bilateral surgery ( $p=0.243$ ). The relative humidity after the choanae decreased from 98.9% to 92.9% after left-sided surgery and decreased to 90.4% after bilateral surgery, with a significant difference between before and after surgery ( $p=0.011$ ). Air temperature after the choanae decreased from 36.6°C to 35.3°C after left-side surgery and to 34.7°C after bilateral surgery, with a significant difference before and after surgery ( $p=0.03$ ).

Wall heat flux in the right nasal cavity increased from 27.1 W/m<sup>2</sup> to 29.1 W/m<sup>2</sup> after left-side surgery and to 74.3 W/m<sup>2</sup> after bilateral surgery, with a significant difference between before and after bilateral surgery ( $p=0.007$ ). Similarly, in the left nasal cavity, wall heat flux increased from 24.9 W/m<sup>2</sup> to 74.2 W/m<sup>2</sup> after left-side surgery and to 71.8 W/m<sup>2</sup> after bilateral surgery, with a significant difference ( $p=0.005$ ). The total wall heat flux also significantly increased from 26.0 W/m<sup>2</sup> (SD: 6.9) before surgery, to 73.0 W/m<sup>2</sup> (SD: 13.5) after bilateral surgery ( $p=0.006$ ). The wall heat flux divided by the airflow rate showed no significant differences before and after surgery, with values of 0.240 (SD: 0.020) before surgery and 0.292 (SD: 0.054) after bilateral surgery ( $p=0.686$ ).

Additionally, Figure 8 summarizes the CFD analysis of the ENS model with respect to the streamline pattern, velocity distribution, relative humidity distribution, wall shear stress, and wall heat flux. The streamlined pattern in the ENS model revealed a more concentrated air distribution, particularly in the middle third of the nasal cavity, in contrast to the relatively even airflow distribution across the upper, middle, and lower parts observed preoperatively. The velocity distribution showed higher airflow velocity at the turbinectomy site. The relative humidity distribution showed that humidity substantially decreased in the lower part of the nasal cavity and choana

after turbinectomy. The wall shear stress greatly increased in the lateral nasal wall area after turbinectomy. Finally, the wall heat flux distribution was significantly influenced in the anterior half of the nasal cavity and choana after turbinectomy.

## DISCUSSION

ENS is a debilitating condition that causes significant suffering in patients, but it is very difficult to conduct patient-oriented research because many of these patients have an emotional aversion towards biopsies or any intervention involving the nose. Consequently, there is limited understanding of its pathophysiology and treatment mechanism until now. To address these issues, our study aimed to develop an ENS model using pigs and validate its relevance through pathological and CFD analysis.

Pigs are widely used as experimental animals because of their physiological similarity to humans. Research on the ENS requires the replication of altered airflow within the nasal cavity, and pigs are among the most suitable animals because of their round nostrils and spacious nasal passages compared to rodents or rabbits, which have a slit-like nostril structure.<sup>19-22</sup> Additionally, pigs are known to frequently develop atrophic rhinitis due to infections, making them a suitable choice for experimental animals.<sup>23</sup> Thus, we chose pigs as experimental animals.

Previous studies on the histological findings of the ENS have been limited and few in number. According to them, squamous metaplasia of the mucosal epithelium, submucosal fibrous scar tissue formation, lymphocyte and plasma cell infiltration, decrease in submucosal glands, goblet cell metaplasia, and atrophic tissue changes can be found in patients with ENS.<sup>2,16,24,25</sup> However, not all of these features are found in every study, and the pathological features vary among patients. Even though there are few studies to compare, according to the largest histologic study until now, involving 17 patients with ENS, revealed significant differences from the control group. Specifically, squamous metaplasia, submucosal fibrosis, and decreased submucosal glands number were observed.<sup>24</sup> From our study, squamous metaplasia

and submucosal fibrosis were significantly increased in the ENS model, which is concordant with a previous study. However, there were observed changes in the number of the submucosal glands, between the ENS group and control. We speculate that the reason for the difference in the submucosal gland number is the difference in the depth of the biopsy. As a human study investigated punch biopsies < 5 mm in size, the involved tissue sometimes did not include a deeper portion of the mucosa. In our study, we harvested the entire nasal mucosa, including the periosteum or perichondrium, and examined the entire mucosal range, from the superficial to the deep layers, to investigate the glands. Owing to squamous metaplasia and submucosal fibrosis in ENS tissues, the superficial part of the mucosa may show a decrease in glands, whereas in the deeper portion, the glands could be preserved. Therefore, we speculate that even though the total number of glands must have decreased because of surgical tissue loss, the number of glands in the remnant tissue might not have changed. Further human studies including deep biopsies are required to confirm these findings.

Even if trigeminal dysfunction is observed in patients with ENS, pathologic changes of the trigeminal nerve have not yet been documented.<sup>11</sup> As a human study had a great obstacle to performing deep biopsy including nerve tissue, while our pig model has ample specimens. We looked for any neural changes, including atrophy or inflammation, but from S-100 staining, we could not find differences from the control side. Based on this, we suspected that functional impairment occurred at the protein level but not through damaged nerve fibers.

TRPM-8 is an ion channel located in C-type sensory nerves, responsible for detecting cold stimuli from the external environment.<sup>26</sup> It is known to play a key role in the perception of airflow by sensing cool temperatures occurring with the evaporation of fluid-lined nasal mucosa. TRPM-8 is also responsive to the perception

of menthol, explaining why individuals experience relief from nasal obstruction when exposed to menthol, even in the absence of any changes in the nasal cavity.<sup>27</sup> Conversely, applying a local anesthetic to the nasal mucosa results in a sensation of nasal congestion.<sup>28</sup> In studies involving menthol lateralization test, patients with ENS have significantly decreased ability to detect menthol, meaning that the impaired sensation of airflow is related to TRPM8.<sup>29,13,14</sup> Previously, it was assumed that in the patients with ENS, the overall amount of TRPM in the mucosa naturally decreased due to overall reduction in mucosal volume.<sup>26,30</sup> However, in experiments staining human nasal mucosa, TRPM8 has been also reported to be expressed in nasal cilia, epithelium, and submucosal glands.<sup>31</sup> Furthermore, in a study involving 17 patients with ENS, mucosal TRPM8 level was significantly decreased compared with that of the control group, which was confirmed by immunohistochemistry of mucosal biopsies.<sup>24</sup> Even though statistically insignificant, our results of TRPM8 level in the mucosa showed generally decreased intensity, in a similar context to the human study. Moreover, our novel findings of decreased TRPM8 levels, especially in the peripheral nerves, indicate that turbinectomy may lead to a decrease in TRPM-8 in the peripheral nerves, which can explain why patients cannot detect cold sensations during breathing, leading to a lack of awareness of airway patency and paradoxical suffocation. It is evident that TRPM-8 stains the neural tissues in the mucosa because it mainly functions as a sensory receptor in nerve fibers. The reason it was not well established in previous human experiments is likely because human tissue samples tend to be limited in quantity, with a predominant focus on studying the epithelium. Further research is needed to determine the reproducibility of these results in humans and the reasons for this phenomenon.

TRPV1 is an ion channel that serves as a pain receptor in peripheral sensory neurons.<sup>32</sup> It is activated by capsaicin, heat, voltage, and acidity.<sup>33</sup> In addition to its

role in pain detection, it has also been found to play a role in thermoregulation, as it can lower body temperature when stimulated.<sup>34</sup> In the human mucosa, TRPV1 is known to be expressed in mucosal epithelium, glands, vascular walls, and mucin.<sup>35</sup> Until recently, there was no attempt to study TRPV1 in the ENS mucosae, but as a member of the TRP family, we assumed that sensory channels other than TRPM8 could also contribute to the pathophysiology of ENS, especially as its function correlates with the symptoms of pain and burning sensation. In our study, we discovered that TRPV1 was also expressed in pig nasal mucosal tissue, especially in the epithelium, glands, vascular walls, and mucin. These findings were consistent with those of previous human studies. Furthermore, we observed a significant increase in TRPV1 levels in the post-turbinectomy side of the mucosa, which can explain the burning sensation symptoms of ENS. Similar increases in TRPV1 levels in mucosa have been described in erosive gastric disease and inflammatory bowel disease, which are believed to contribute to the heightened pain sensitivity in those patients.<sup>36,37</sup> Since inflammation is known to induce the overexpression of TRPV1, this change in TRPV1 levels in the ENS model mucosa may be attributed to tissue inflammation caused by altered airflow.<sup>38</sup> Given that there have been efforts to use TRPV1 agonists and antagonists for therapeutic pain control, further studies utilizing these agents could be considered as potential treatments for ENS symptoms.<sup>39,40</sup>

PIEZO-2 is a pressure receptor present in somatosensory neurons and Merkel cells, allowing it to detect light touch and proprioception.<sup>41</sup> It functions as a mechanoreceptor in various organs and plays a crucial role in sensing air pressure and controlling respiration in the respiratory tract.<sup>42</sup> In laboratory tests, newborn mice with PIEZO-2 knockout suffer from respiratory distress and often do not survive, while individuals with a congenital deficiency of PIEZO-2 require respiratory support immediately after birth and may experience shallow breathing

throughout their lives.<sup>43,44</sup> As nasal resistance significantly changes in patients with ENS, we speculated that it is worth examining whether PIEZO-2 levels also change in our ENS model. However, no studies have investigated the relationship between PIEZO-2 and the nasal mucosa, highlighting the need for further research in this field. Our study revealed that PIEZO-2 is primarily expressed in capillary endothelial cells rather than in neurons, suggesting that PIEZO-2 has more potential connections with mucosal swelling, whereas, in the trigeminal nerve, it does not play as significant a role as it does in the lungs.

Recent studies on ENS using CFD techniques have gained momentum. In studies conducted on human participants, it was observed that patients with severe turbinate resection showed associations with ENS through CFD analysis.<sup>12</sup> In another study involving patients with ENS, nasal flow rates were significantly higher at 173.1 mL/s, compared to the normal control group with a rate of 116.0 mL/s. This aligns with the results of our study, where nasal flow rates increased from 107.6 mL/s before surgery to 250.0 mL/s after surgery.<sup>13</sup> A study examining choanal air temperature in turbinate removal patients also found a decrease in air temperature in surgical patients, which is consistent with our findings.<sup>45,46</sup> Another study calculating nasal resistance in patients with ENS confirmed a significant reduction in nasal resistance, consistent with our research.<sup>47</sup> Through the above results, the utility of our model has been supported through a CFD study.

Another finding from the CFD study of patients with ENS is that an altered airflow pattern is an important factor in the development of ENS symptoms. The existing hypotheses suggest that ENS is more likely to occur when wall shear stress of the olfactory mucosa decreases and airflow distribution to the nasal floor decreases.<sup>10</sup> Also, according to the study by Malik et al., comparing CFD airflow patterns of patients who developed ENS and those who did not, after an aggressive turbinate

surgery, nasal resistance was similar in both groups, but a particularly decreased inferior flow was observed in the ENS group.<sup>14</sup> We also observed a similar pattern in our porcine model where airflow converged in the middle and decreased in both upper and lower regions, further confirming the validity of the ENS model.

There are some limitations to our study. First, we could not estimate the symptoms in our animal subjects. This is a significant limitation because ENS is defined by the symptoms experienced by patients. However, in the animal model of total turbinectomy, we discovered previously unknown factors and observed histological and flow-dynamic changes after the procedure. We do not know whether our pigs suffered many ENS symptoms because all of them showed normal behavior and growth after the surgeries. Even so, if turbinectomy itself makes certain changes to the nasal cavity regardless of the presence of ENS symptoms, and if we can measure the damage and restoration by certain means, this animal model will serve as a great tool to elucidate the pathogenesis and develop treatment for ENS. Second, there are certain anatomical differences between swine and humans, which can make the practicality of the disease model less plausible. Pig noses are much longer from front to back than humans, providing more protection against ENS development. If the nasal cavity is longer, it provides more opportunities for the air to become more conditioned until it reaches the choana. However, despite this drawback, our swine model showed significant differences between preoperative and postoperative findings, confirming its significant potential as a feasible animal model. However, further studies are required to confirm these findings.

## **CONCLUSION**

This study holds significance as it is the first animal model for ENS. Through this model, it was observed that the TRPM-8 levels in the nerve tissues decreased and the TRPV1 levels in the mucosa increased following turbinectomy, which may explain the decreased cooling sensation of airflow and burning sensation in patients with ENS. Additionally, the CFD analysis of this model showed similar patterns of changes in nasal flow, temperature, and humidity that corresponded to those observed in patients with ENS. This new model is expected to help elucidate the pathophysiology of ENS and aid the development of treatment strategies.

## REFERENCES

1. Huang CC, Wu PW, Lee CC, Huang CC, Fu CH, Chang PH, et al. Comparison of SNOT-25 and ENS6Q in evaluating patients with empty nose syndrome. *Laryngoscope Investig Otolaryngol.* 2022;7(2):342-348.
2. Dzhankov DL, Stoyanov GS, Georgiev R, et al. Histopathological findings in an unclassifiable case of empty-nose syndrome with long-term follow-up. *Cureus.* 2018;10(5):e2655.
3. Sozansky J, Houser SM. Pathophysiology of empty nose syndrome. *Laryngoscope.* 2015;125(1):70-74.
4. Huang CC, Wu PW, Lee CC, Chang PH, Huang CC, Lee TJ. Suicidal thoughts in patients with empty nose syndrome. *Laryngoscope Investig Otolaryngol.* 2022;7(1):22-28.
5. Di Girolamo S. Atrophic rhinitis: from the voluptuary nasal pathology to empty nose syndrome. Springer International Publishing, 2020.
6. Keime-Guibert F, Napolitano M, Delattre JY. Neurological complications of radiotherapy and chemotherapy. *J Neurol.* 1998;245(11):695-708.
7. Yuk J, Akash MMH, Chakraborty A, Basu S, Chamorro LP, Jung S. Morphology of pig nasal structure and modulation of airflow and basic thermal conditioning. *Integr Comp Biol.* 2023;63(2):304-314.
8. Liu Y, Mikrani R, He Y, Faran Ashraf Baig MM, Abbas M, Naveed M, et al. TRPM8 channels: A review of distribution and clinical role. *Eur J Pharmacol.* 2020;882:173312.
9. McKemy DD, Neuhauser WM, Julius D. Identification of a cold receptor reveals a general role for TRP channels in thermosensation. *Nature.*

2002;416(6876):52-58.

10. Ji RR, Lee SY. Molecular sensors of temperature, pressure, and pain with special focus on TRPV1, TRPM8, and PIEZO2 ion channels. *Neurosci Bull.* 2021;37(12):1745-1749.

11. Earley S, Santana LF, Lederer WJ. The physiological sensor channels TRP and piezo: Nobel Prize in Physiology or Medicine 2021. *Physiol Rev.* 2022;102(2):1153-1158.

12. Huang AN, Chen WC, Wu CL, Lee TJ, Huang CC, Kuo H. Characterization of nasal aerodynamics and air conditioning ability using CFD and its application to improve the empty nose syndrome (ENS) submucosal floor implant surgery – Part I methodology. *J Taiwan Inst Chem Eng.* 2022;138:104481.

13. Li C, Farag AA, Leach J, Deshpande B, Jacobowitz A, Kim K, et al. Computational fluid dynamics and trigeminal sensory examinations of empty nose syndrome patients. *Laryngoscope.* 2017;127(6):E176-E184.

14. Malik J, Li C, Maza G, Farag AA, Krebs JP, McGhee S, et al. Computational fluid dynamic analysis of aggressive turbinate reductions: is it a culprit of empty nose syndrome? *Int Forum Allergy Rhinol.* 2019;9(8):891-899.

15. Kim DW, Chung SK, Na Y. Numerical study on the air-conditioning characteristics of the human nasal cavity. *Comput Biol Med.* 2017;86:18-30.

16. Moore EJ, Kern EB. Atrophic rhinitis: a review of 242 cases. *Am J Rhinol.* 2001;15(6):355-361.

17. Chung SK, Na Y. Dynamic characteristics of heat capacity of the human nasal cavity during a respiratory cycle. *Respir Physiol Neurobiol.* 2021;290:103674.

18. Lindemann J, Leiacker R, Rettinger G, Keck T. Nasal mucosal temperature during respiration. *Clin Otolaryngol Allied Sci.* 2002;27(3):135-139.

19. Moshkin MP, Petrovskii DV, Akulov AE, Romashchenko AV, Gerlinskaia LA, Muchnaia MI, et al. Aerosol deposition in nasal passages of burrowing and ground rodents when breathing dust-laden air. *Zh Obshch Biol.* 2014;75(3):214-225.
20. Xi J, Si XA, Kim J, Zhang Y, Jacob RE, Kabilan S, et al. Anatomical Details of the Rabbit Nasal Passages and Their Implications in Breathing, Air Conditioning, and Olfaction. *Anat Rec.* 2016;299(7):853-868.
21. Karthik K, Chakraborty S, Banik S. Muzzle Analysis for Biometric Identification of Pigs. In: 2017 Ninth International Conference on Advances in Pattern Recognition (ICAPR). IEEE; 2017. doi:10.1109/icapr.2017.8593204
22. Xi J, Talaat M, Si X, Dong H, Donepudi R, Kabilan S, et al. Ventilation Modulation and Nanoparticle Deposition in Respiratory and Olfactory Regions of Rabbit Nose. *Animals (Basel).* 2019;9(12). doi:10.3390/ani9121107
23. Magyar T, Lax AJ. Atrophic Rhinitis. In: *Polymicrobial Diseases.* ASM Press; 2014:169-197.
24. Wu CL, Fu CH, Lee TJ. Distinct histopathological characteristics in empty nose syndrome. *Laryngoscope.* 2021;131(1):E14-E18.
25. Dholakia SS, Grimm D, Daum R, Bravo DT, Salvi N, Zarabanda D, et al. The Serpentine Sign: A Reliable Endoscopic and Radiographic Finding in Empty Nose Syndrome. *Laryngoscope.* Published online September 13, 2023. doi:10.1002/lary.30938
26. Iftinca M, Altier C. The cool things to know about TRPM8 Channels. 2020;14(1):413-420.
27. Zhao K, Jiang J, Blacker K, Lyman B, Dalton P, Cowart BJ, et al. Regional peak mucosal cooling predicts the perception of nasal patency. *Laryngoscope.* 2014;124(3):589-595.
28. Eccles R, Morris S, Tolley NS. The effects of nasal anaesthesia upon nasal

sensation of airflow. *Acta Otolaryngol.* 1988;106(1-2):152-155.

29. Konstantinidis I, Tsakiropoulou E, Chatziavramidis A, Ikonmidis C, Markou K. Intranasal trigeminal function in patients with empty nose syndrome. *Laryngoscope.* 2017;127(6):1263-1267.

30. Gordiienko IM, Gubar OS, Sulik R, Kunakh T, Zlatskiy I, Zlatska A. Empty nose syndrome pathogenesis and cell-based biotechnology products as a new option for treatment. *World J Stem Cells.* 2021;13(9):1293-1306.

31. Liu SC, Lu HH, Cheng LH, Chu YH, Lee FP, Wu CC, et al. Identification of the cold receptor TRPM8 in the nasal mucosa. *Am J Rhinol Allergy.* 2015;29(4):e112-e116.

32. Bevan S, Quallo T, Andersson DA. TRPV1. *Handb Exp Pharmacol.* 2014;222:207-245.

33. Tominaga M, Tominaga T. Structure and function of TRPV1. *Pflugers Arch.* 2005;451(1):143-150.

34. Gavva NR. Bodytemperature maintenance is the predominant function of the vanilloid receptor TRPV1. *Trends Pharmacol Sci.* 2008;29(11):550-557.

35. Seki N, Shirasaki H, Kikuchi M, Sakamoto T, Watanabe N, Himi T. Expression and localization of TRPV1 in human nasal mucosa. *Rhinology.* 2006;44(2):128-134.

36. Guarino MPL, Cheng L, Ma J, Harnett K, Biancani P, Altomare A, et al. Increased TRPV1 gene expression in esophageal mucosa of patients with non-erosive and erosive reflux disease. *Neurogastroenterol Motil.* 2010;22(7):746-751, e219.

37. Akbar A, Yiangou Y, Facer P, Walters JRF, Anand P, Ghosh S. Increased capsaicin receptor TRPV1-expressing sensory fibres in irritable bowel syndrome and their correlation with abdominal pain. *Gut.* 2008;57(7):923-929.

38. Lee LY, Gu Q. Role of TRPV1 in inflammation-induced airway

hypersensitivity. *Curr Opin Pharmacol.* 2009;9(3):243-249.

39. Duarte Y, Cáceres J, Sepúlveda RV, Arriagada D, Olivares P, Díaz-Franulic, et al. Novel TRPV1 Channel Agonists With Faster and More Potent Analgesic Properties Than Capsaicin. *Front Pharmacol.* 2020;11:1040.

40. Knotkova H, Pappagallo M, Szallasi A. Capsaicin (TRPV1 Agonist) therapy for pain relief: farewell or revival? *Clin J Pain.* 2008;24(2):142-154.

41. Chesler AT, Szczot M, Bharucha-Goebel D, Čeko M, Donkervoort S, Laubacher C, et al. The Role of PIEZO2 in Human Mechanosensation. *N Engl J Med.* 2016;375(14):1355-1364.

42. Szczot M, Nickolls AR, Lam RM, Chesler AT. The form and function of PIEZO2. *Annu Rev Biochem.* 2021;90(1):507-534.

43. Alper SL. Genetic Diseases of PIEZO1 and PIEZO2 Dysfunction. *Curr Top Membr.* 2017;79:97-134.

44. Nonomura K, Woo SH, Chang RB, Gillich A, Qiu Z, Francisco AG, et al. Piezo2 senses airway stretch and mediates lung inflation-induced apnoea. *Nature.* 2017;541(7636):176-181.

45. Scheithauer MO. Surgery of the turbinates and “empty-nose syndrome. *GMS Curr Top Otorhinolaryngol Head Neck Surg.* 2010;9:Doc03.

46. Lindemann J, Keck T, Wiesmiller KM, Rettinger G, Brambs HJ, Pless D. Numerical simulation of intranasal air flow and temperature after resection of the turbinates. *Rhinology.* 2005;43(1):24-28.

47. Di MY, Jiang Z, Gao ZQ, Li Z, An YR, Lv W. Numerical simulation of airflow fields in two typical nasal structures of empty nose syndrome: a computational fluid dynamics study. *PLoS One.* 2013;8(12):e84243.

**Table 1.** Summary of histological findings of hematoxylin and eosin staining.

| Histologic findings                                  | Site          | ENS model<br>n (%), N=28 | Control<br>n (%), N=28* | <i>P</i>     |
|--|---------------|--------------------------|-------------------------|--------------|
| Squamous metaplasia<br>(0=not present, 1=present)    |               |                          |                         |              |
|  | Anterior      | 27 (96.4)                | 22 (78.6)               | <b>0.043</b> |
|  | Middle        | 8 (28.5)                 | 6 (21.4)                | 0.537        |
|  | Posterior     | 0 (0)                    | 3 (10.7)                | 0.075        |
|  | Sum (n, N=84) | 48 (57.1)                | 32 (38.1)               | 0.147        |
| Chronic inflammation<br>(0=not present, 1=present)   |               |                          |                         |              |
|  | Anterior      | 6 (21.4)                 | 8(28.5)                 | 0.537        |
|  | Middle        | 13 (46.4)                | 9 (32.1)                | 0.274        |
|  | Posterior     | 14 (50.0)                | 21 (75.0)               | 0.053        |
|  | Sum (n, N=84) | 33 (39.3)                | 38 (45.2)               | 0.435        |
| Submucosal fibrosis<br>(0=not present, 1=present)    |               |                          |                         |              |
|  | Anterior      | 4 (14.3)                 | 2 (7.1)                 | 0.388        |
|  | Middle        | 12 (42.9)                | 5 (17.9)                | <b>0.018</b> |
|  | Posterior     | 8 (28.6)                 | 9 (32.1)                | 0.084        |
|  | Sum (n, N=84) | 48 (57.1)                | 32 (38.1)               | 0.147        |
| Submucosal gland<br>(0=less than 25%, 1=25% or more) |               |                          |                         |              |
|  | Anterior      | 16 (57.1)                | 13 (46.4)               | 0.422        |
|  | Middle        | 11(39.3)                 | 13 (46.4)               | 0.644        |
|  | Posterior     | 5 (17.9)                 | 2 (7.1)                 | 0.225        |
|  | Sum (n, N=84) | 32 (38.1)                | 28 (33.3)               | 0.520        |
| Atrophic change<br>(0=not present, 1=present)        |               |                          |                         |              |
|  | Anterior      | 1(3.6)                   | 0 (0)                   | 0.313        |
|  | Middle        | 6 (21.4)                 | 11(39.3)                | 0.146        |
|  | Posterior     | 15 (53.6)                | 15 (53.6)               | NA           |
|  | Sum (n, N=84) | 22 (78.6)                | 26 (40.0)               | 0.494        |

**Table 2.** Summary of quantitative immunohistochemical analysis.

|         | Intensity (mean, 0~300) |         |       | Nerve stain (mean, %) |         |              |
|---------|-------------------------|---------|-------|-----------------------|---------|--------------|
|         | ENS                     | Control | P     | ENS                   | Control | P            |
| TRPM8   | 111.4                   | 146.3   | 0.373 | 50.0                  | 95.3    | <b>0.010</b> |
| TRPV1   | 189.9                   | 153.7   | 0.373 | 71.4                  | 14.3    | <b>0.025</b> |
| PIEZO-2 | 171.7                   | 100.6   | 0.126 | 10.7                  | 0       | 0.406        |

The Mann–Whitney U test was used to calculate p values,  $p < 0.05$  is considered a statistically significant.

**Table 3.** Preoperative and postoperative CFD calculation data.

| <b>variables</b>                   | <b>Pre-op<br/>Mean (SD)</b> | <b>Post-op<br/>(Left)<br/>Mean (SD)</b> | <b>Post-op<br/>(Both)<br/>Mean (SD)</b> | <b>P</b>         |
|------------------------------------|-----------------------------|---|---|------------------|
| Airflow rate, nostril, R (mL/s)    | 55.6(13.1)                  | 57.2(12.2)                              | 130.1(10.8)                             | <b>0.002</b>     |
| Airflow rate, nostril, L (mL/s)    | 53.3(9.5)                   | 127.3(14.8)                             | 121.8(10.7)                             | <b>0.001</b>     |
| Flow partition, R : L (%)          | 50.7:49.3(3.0)              | 31.1:69.0(6.5)                          | 51.6:48.3(4.2)                          | 0.778            |
| Airflow rate, inlet (mL/s)         | 107.6(22.0)                 | 182.9(9.4)                              | 250.0(0.3)                              | <b>&lt;0.001</b> |
| Unilateral NR, R (Pa s/mL)         | 0.154(0.096)                | 0.146(0.089)                            | 0.155(0.024)                            | 0.987            |
| Unilateral NR, L (Pa s/mL)         | 0.148(0.074)                | 0.053(0.015)                            | 0.052(0.013)                            | 0.091            |
| Bilateral NR (Pa s/mL)             | 0.077(0.043)                | 0.041(0.015)                            | 0.030(0.012)                            | 0.243            |
| RH after choanae (%)               | 98.9(0.9)                   | 92.9(0.9)                               | 90.4(3.2)                               | <b>0.011</b>     |
| Air T after choanae (°C)           | 36.6(0.1)                   | 35.3(0.2)                               | 34.7(0.5)                               | <b>0.003</b>     |
| WHF, cavity, R (W/m <sup>2</sup> ) | 27.1(7.5)                   | 29.1(7.7)                               | 74.3(14.7)                              | <b>0.007</b>     |
| WHF, cavity, L (W/m <sup>2</sup> ) | 24.9(6.4)                   | 74.2(12.4)                              | 71.8(13.1)                              | <b>0.005</b>     |
| WHF, total (W/m <sup>2</sup> )     | 26.0(6.9)                   | 48.9(6.9)                               | 73.0(13.5)                              | <b>0.006</b>     |
| WHF/ (airflow rate)                | 0.240(0.020)                | 0.262(0.020)                            | 0.292(0.054)                            | 0.686            |

A t-test was performed to compare the preoperative and postoperative (both) mean values,  $p < 0.05$  is considered as a statistically significant value.

Abbreviations: NR, nasal resistance; RH, relative humidity; T, temperature; WHF, wall heat flux

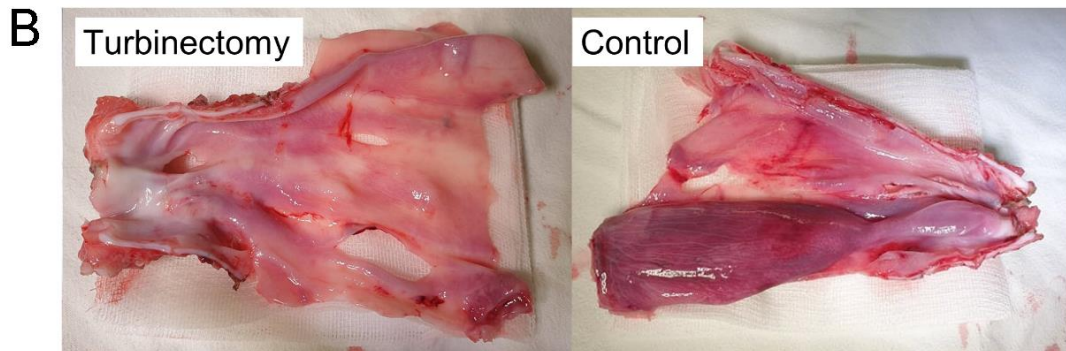


**Figure 1.** A: Surgical view after harvesting the mucosa. B: Mucosal side of harvested specimens: post-turbineotomy site and control.

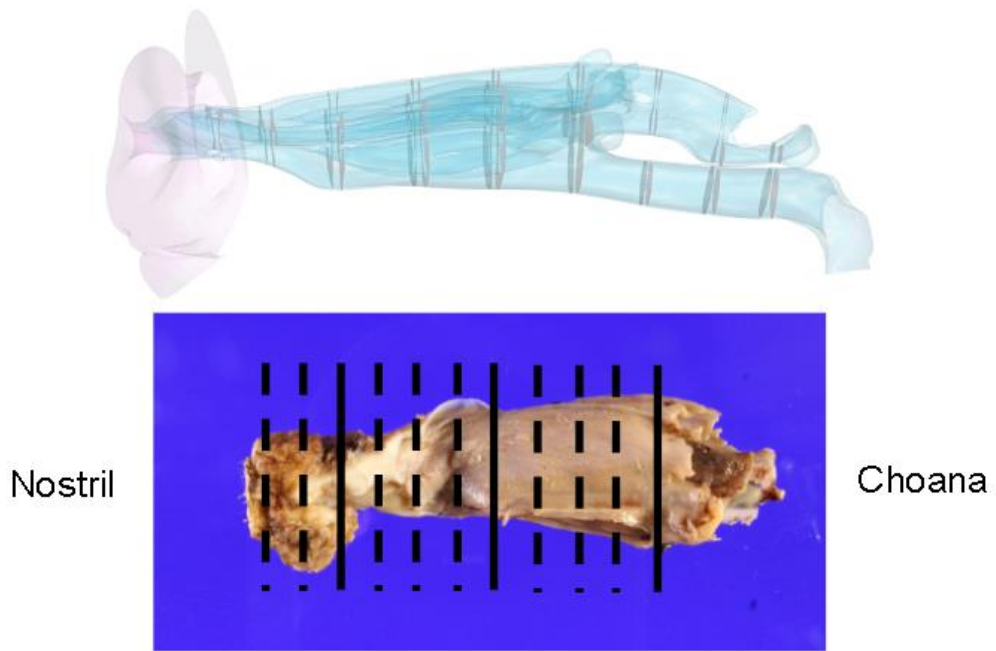


**Figure 2.** When the entire nasal mucosal specimen was harvested in a cylindrical shape, vertical sections were prepared for correlation with the coronal section of the CT scan.

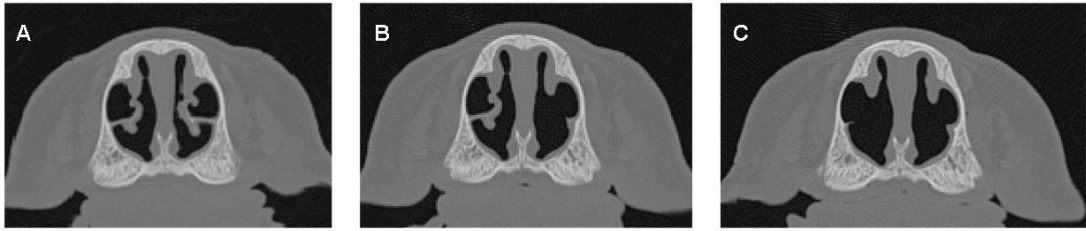


**Figure 3.** CT scan of a pig head. (A) Preoperative, (B) after left side unilateral inferior turbinectomy, (C) after bilateral inferior turbinectomy.

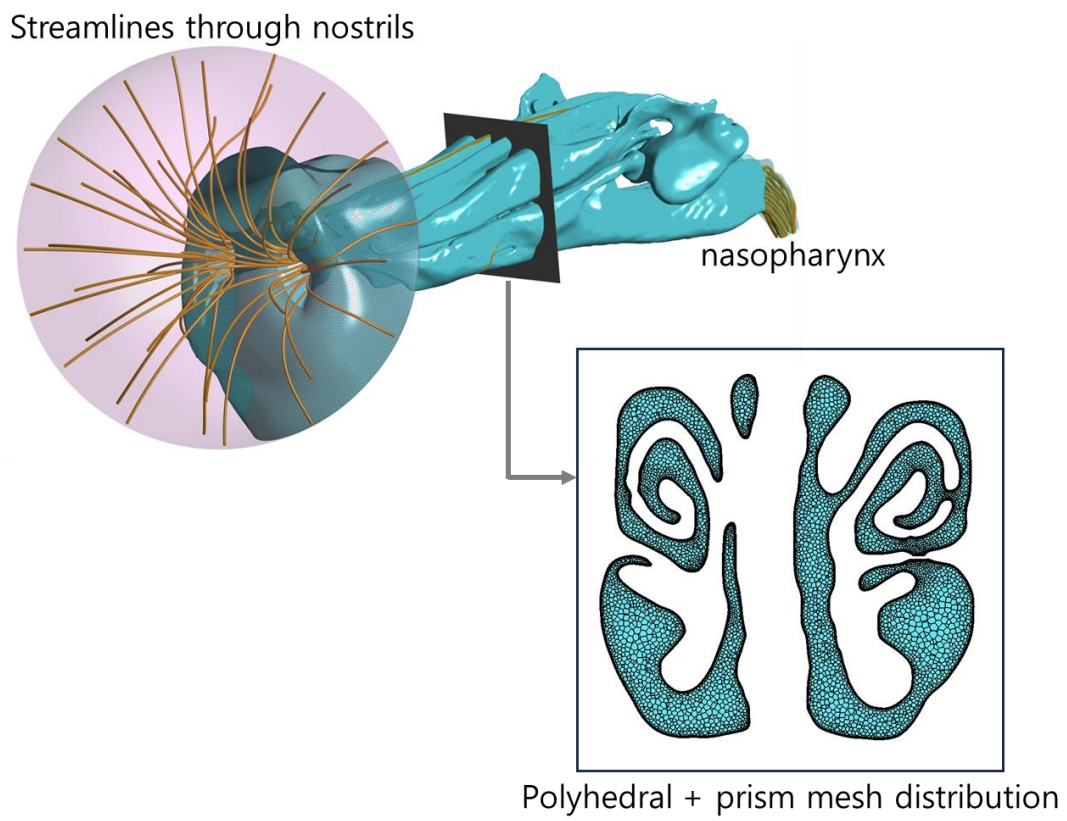


**Figure 4.** Numerical nasal cavity model.

H&E : Control

H&E : ENS Model

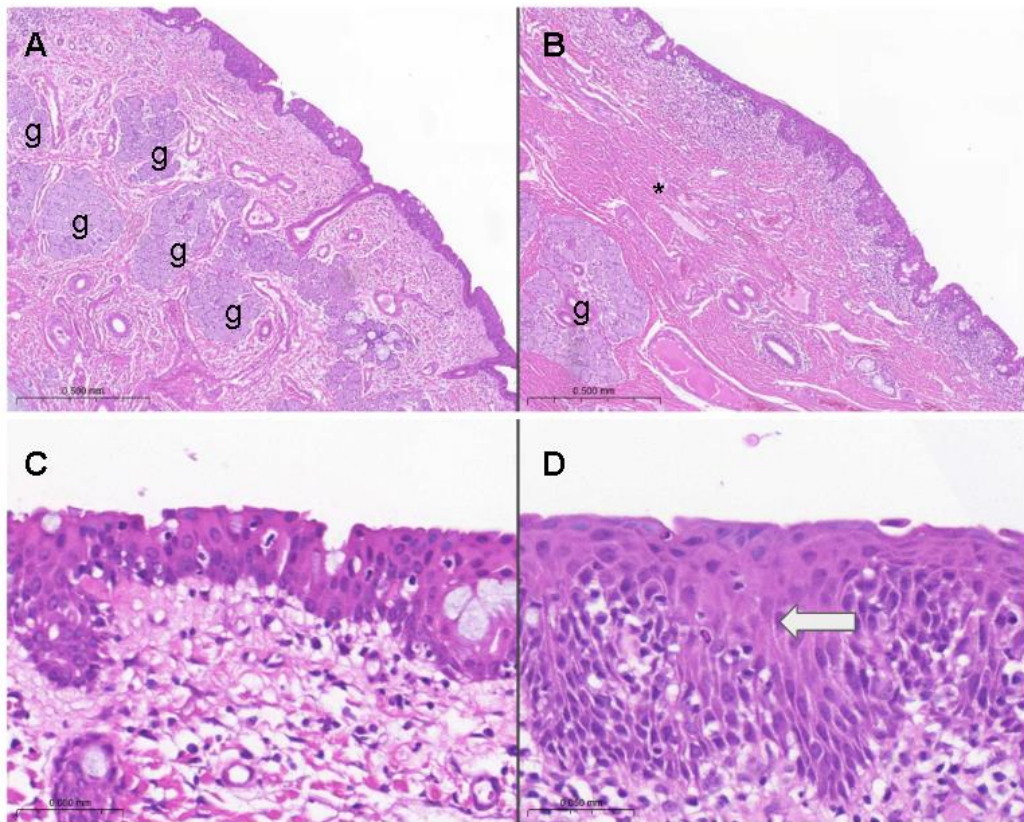


**Figure 5.** H&E-stained specimens of control (A, C) and ENS group. (B, D) In the lower-power view, the ENS group showed decreased mucosal glands (g) and submucosal fibrosis (asterisk) compared to the control group. (B) The mucosal lining of the ENS group was thickened and showed prominent squamous metaplasia. (D, arrow)

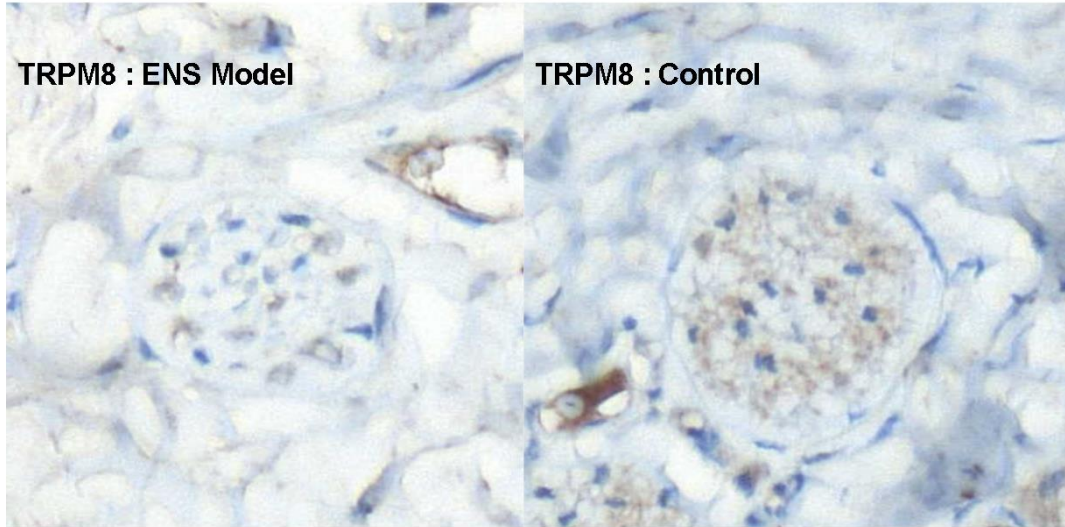


**Figure 6.** TRPM-8 levels in the peripheral nerves were decreased, whereas they were present in the small nerves of the control group.

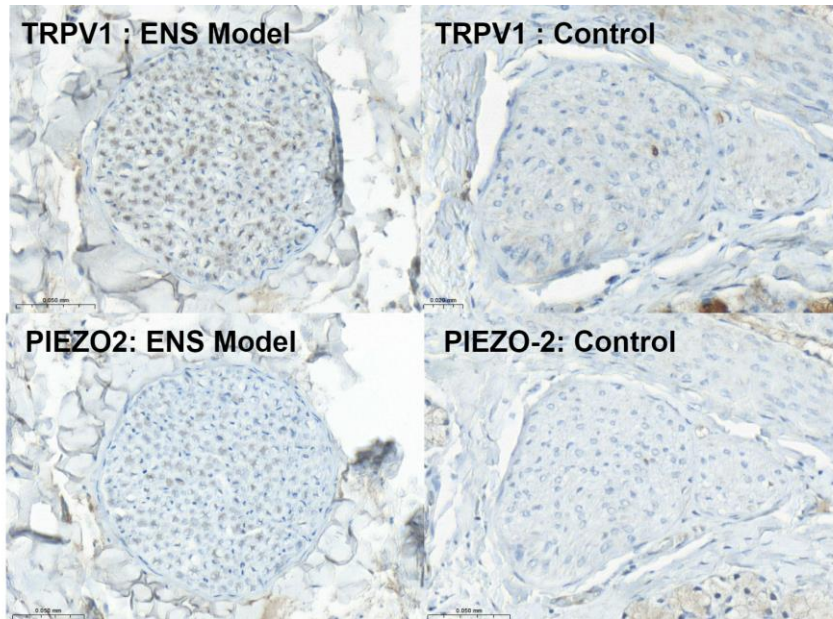


**Figure 7.** Comparison of TRPV1 and PIEZO-2 levels in control and ENS models. TRPV1 staining was prominent in the cytoplasm of ENS model nerve fibers. PIEZO-2 staining was mildly increased in the cytoplasm of ENS model nerve fibers.

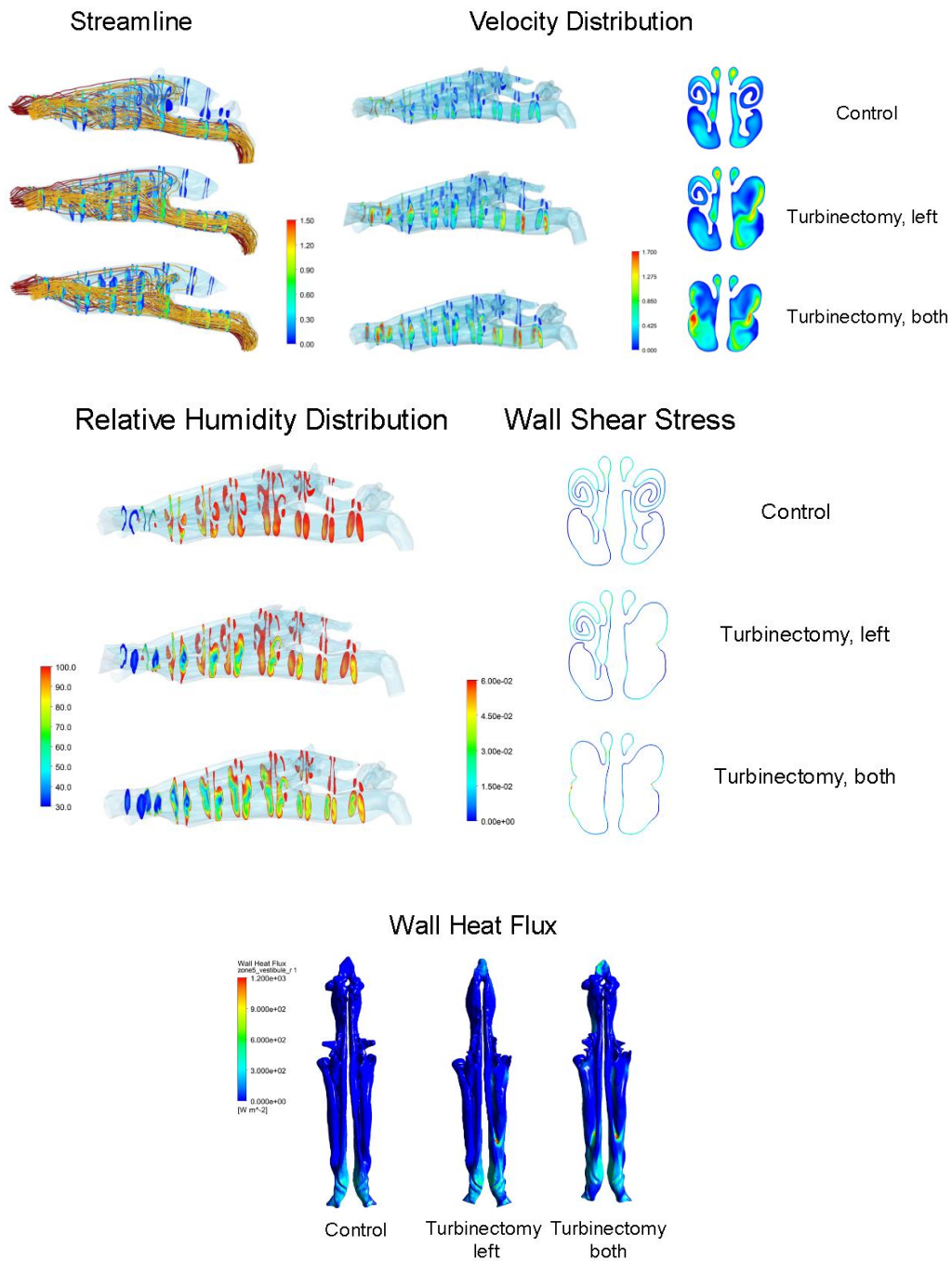


**Figure 8.** CFD analysis of the ENS model regarding streamline pattern, velocity distribution, relative humidity distribution, wall shear stress, and wall heat flux. The ENS model showed airflow centered in the middle third of the nasal cavity, increased air velocity throughout the nasal passage, especially in the middle third, decreased relative humidity, increased wall shear stress, and increased wall heat flux.

## 국문요약

**배경 및 목적:** 빈코 증후군은 하비갑개 수술 이후 발생하는 의인성 질환으로, 환자들이 호소하는 고통은 심한데 비해 질병 발생의 원인이나 치료에 대해서는 아직 밝혀진 바가 많지 더 광범위한 기초 연구가 필요한 분야이다. 아직까지 빈코 증후군의 동물모델이 전무한 현실이나, 잘 확립된 동물 모델은 복잡한 질환의 병인을 더 잘 이해하고 치료법을 개발할 기반이 될 것이다. 따라서 본 연구는 빈코 증후군의 돼지 모델을 개발하고 이 모델의 실현 가능성을 조직학 및 계산 유체 역학 분석을 통해 확인하고자 한다.

**방법:** 총 4 마리의 Yorkshire 돼지에 좌측 하비갑개 전절제를 시행한 후 6 개월 후 희생하였다. 양쪽 비점막 전체를 채취하여 H&E 염색, S-100 염색, TRPM-8 수용체 염색, TRPV1 및 PIEZO-2 염색을 사용하여 조직학적 분석을 실시하였다. 또한, 돼지 비강의 컴퓨터 단층 촬영을 이용한 계산 유체 역학 분석을 수행하여 기능적 측면에서 질병 모델을 검증하였다. 돼지 비강의 컴퓨터 단층 촬영은 수술 전, 좌측 하비갑개 절제 후 및 양측 하비갑개 절제 후에 각각 시행되었다.

**결과:** H&E 염색은 빈코 증후군 돼지 모델의 비강 전반부에서 편평상피 화생이 유의적으로 증가함을 보여주었다 (양성률 96.4% 대 78.6%,  $p=0.043$ ). 또한 비강 중반부에서 점막 하 섬유화가 유의하게 증가하였다

(양성률 42.9% 대 17.9%,  $p=0.018$ ). S-100 염색에서는 신경 주위의 염증이나 변화는 없었지만 신경에서 TRPM-8 발현이 현저히 감소함을 보여주었다 (양성률 50.0% 대 95.3%,  $p=0.010$ ). TRPV1 발현은 전반적으로 증가하고 신경에서의 발현률이 증가하였다 (양성률 71.4% 대 14.3%,  $p=0.025$ ). 계산 유체 역학 분석 결과, 빈코 증후군 돼지 모델에서 전반적인 기류 저항이 감소하고, 비인두에서 상대 습도 및 공기 온도가 감소하는 것을 보여주었다, 이는 실제 빈코 증후군 환자에서의 변화와 유사하다.

**결론:** 돼지를 이용한 빈코 증후군 동물 모델에 대한 조직학적 검사와 계산 유체 역학 결과는 본 모델이 빈코 증후군의 실현 가능한 동물 모델로 기능할 수 있음을 보여준다.